Research article

Insights into the binding of buspirone to human serum albumin using multi-spectroscopic and molecular docking techniques

Javad Sargolzaei [a],[*],[1], Elaheh Jalali [a],[1], Parisa Rajabi [b]

[a] *Department of Biology, Faculty of Science, Arak University, Arak, 38156-8-8349, Iran*
[b] *Department of Psychiatry, Arak University of Medical Sciences, Arak, Iran*

A B S T R A C T

Buspirone is an anxiolytic drug that plays a significant role in managing anxiety disorders and alleviating their symptoms as well. Several techniques were utilized to study the interaction between buspirone and human serum albumin under physiological conditions, including UV–vis absorption spectroscopy, fluorescence emission spectroscopy, circular dichroism, Fourier transform infrared spectroscopy (FT-IR), equilibrium dialysis, and molecular docking. The results of this study demonstrated that buspirone quenched the intrinsic fluorescence of human serum albumin through a mixed mechanism. Moreover, the binding constants (K_b), the quenching constants (K_{sv}), and thermodynamic parameters were calculated at various temperatures. The binding process of buspirone to human serum albumin showed a cooperative binding pattern, confirmed by the Scatchard diagram and Hill coefficient. Molecular docking results showed that buspirone interacted with the IIA, IIIA, and IIB subdomains of human serum albumin and slightly changed its conformation. It was also found that hydrophobic forces played a major role in this interaction. This study consequently proves that BSH as a drug can be transported by blood albumin. Additionally, due to its ratiometric response in absorbance upon binding to a biological target, HSA can be used as a molecular probe to follow biomolecular interactions.

1. Introduction

Buspirone hydrochloride (BSH), an azaspirodecanedione compound, is an anxiolytic drug and partial serotonin receptor agonist used to manage anxiety disorders and alleviate symptoms [1,2]. It seems that its anxiolytic effects are related to its effect on the neurotransmitter serotonin (5-HT) [3]. It should be mentioned that treatment with this drug is associated with several common side effects, such as headache, dizziness, nausea, and difficulty concentrating [4].

Albumin is the main component of plasma proteins and its structure is suitable for binding and transporting ligands [5]. It is widely known that drugs can bind to human serum albumin (HSA), producing both therapeutic effects and side effects. HSA, which accounts for approximately 60 % of all plasma, has a crucial function in the transport of various substances including drugs [6,7]. The binding of the drug to HSA may affect its metabolism and its distribution [8,9]. HSA is composed of a single polypeptide chain of 585 amino acids with three homologous domains arranged asymmetrically and forming a heart shape. The essential binding sites for drugs in this protein are Sudlow's site I (subdomain IIA) and Sudlow's site II (subdomain IIIA). However, it is believed that site III (subdomain IB)

---

* Corresponding author.
 E-mail address: j-sargolzaei@araku.ac.ir (J. Sargolzaei).
[1] These authors contributed equally as the first author.

also plays an essential role in the binding of various drugs [10]. It has been found that buspirone hydrochloride (BSH) can interact with HSA and can cause changes in its biochemical response to other molecules [11–13].

The current research was conducted with the aim of obtaining detailed information about the binding sites, fluorescence quenching mechanism of HSA, the binding constant (K_b), binding mode, microenvironmental changes, and the structure of HSA. The results of this study are expected to shed light on the mechanism of action and pharmacokinetic and pharmacodynamic properties of BSH as well.

2. Materials and methods

2.1. Reagents and solutions

Buspirone hydrochloride ($\geq$99.5 %) was purchased from Tehran Daru Company. HSA (fraction V, $\geq$99.0 %), sodium dihydrogen phosphate ($NaH_2PO_4 \cdot 2H_2O$, $\geq$99.0 %), and disodium hydrogen phosphate ($Na_2HPO_4 \cdot 2H_2O$, $\geq$99.0 %) were also purchased from Sigma-Aldrich.

The phosphate-buffered saline (PBS) containing NaH_2PO_4 and Na_2HPO_4 was prepared in double-distilled water and adjusted to pH 7.4 using NaOH/HCl. Buspirone stock solution (4×10^{-3} M) and HSA (75×10^{-6} M) were prepared in deionized water. Then, the solutions were stored at 4 °C. It should be mentioned that all the sample solutions were diluted using PBS 20 mM. Also, all experiments were repeated three times, and their averages were reported as well.

2.2. UV–vis spectroscopy

The UV–vis spectra of HSA and BSH were measured at pH 7.4 using an SCO spectrophotometer with a 1 mm quartz cell, covering the range of 190–700 nm. It should be noted that the absorbance of BSH at each point was subtracted from the absorbance of BSH-HSA complex and the results were reported.

2.3. Fluorescence spectroscopy

In this study, solutions of HSA in the absence and presence of various concentrations of BSH (0–200 μM) were incubated at three different temperatures (298, 303,308, and 312 K) in the dark for 1 h. The fluorescence emission spectra were obtained in the range of 300–450 nm on a Cary Eclipse fluorescence spectrometer (Varian) with thermostatic control. The slit widths of the excitation and emission were set to 5 nm. Excitation was performed at 295 nm wavelength. The spectra of different BSH concentrations were recorded under the same conditions for background correction.

2.4. The inner filter effects

The phenomenon known as the inner-filter effect refers to the absorption of the component added during a fluorescence titration experiment at the wavelength of excitation or emission. This absorption results in a factitious reduction in the observed fluorescence intensity [14]. In the context of steady-state fluorescence experiments, the absorption spectrum of BSH exhibits an overlap with both the excitation and emission spectra of HSA. Thus, it is crucial to subtract such an effect from the raw quenching data. The fluorescence data was corrected for inner filter effect using Eq. (1):

$$F_{corr} = F_{obs} \, antilog \left[(A_{em} + A_{ex}) \right] / 2 \tag{1}$$

where F_{obs} and F_{corr} are the observed and corrected fluorescence intensity, A_{em} and A_{ex} are the absorbances of the sample at the emission and excitation wavelengths, respectively.

2.5. Circular dichroism

The circular dichroism (CD) spectra of HSA solutions with different concentrations of BSH were obtained using an AVIV-215 spectrometer. Measurements were performed in the range of 190–260 nm with scan speed of 20 nm/min and a response time of 0.3330 s at room temperature (297 $\pm$ 2 K). The spectra of different concentrations of BSH under the same conditions were measured and used for background correction. The obtained data were analyzed using a quantitative multivariate analysis program on an AVIV-215 CD spectrometer to determine the secondary structure of the protein in the absence and presence of BSH.

2.6. FT-IR measurements

The FT-IR spectra of HSA and BSH solutions were recorded using an alpha spectrometer in the range of 1000–4000 cm^{-1}. First of all, the amount of absorption of HSA and BSH was recorded separately. It is worth mentioning that the concentration of HSA in all solutions was fixed at 100 μM. Then, the spectrum of the BSH-HSA solution was measured with a molar ratio of 1:0.5 and 1:1 protein-ligand. The absorption rate of free BSH was subtracted from the absorption rate of BSH-HSA and the obtained results were eventually reported.

2.7. Equilibrium dialysis

HSA and BSH were prepared in PBS at pH 7.4 and Dialysis tubing cellulose membrane (molecular weight cut off = 10,000 Da) was purchased from Scientific Instrument Center (SIC, China). HSA was dialyzed against the same buffer with various concentrations of BSH using Spectrum Laboratories dialysis tubing at room temperature (297 ± 2 K). The equilibrium was reached within 72 h. The free drug concentration (C_f) and total drug concentration (C_t) in dialysis before and after dialysis were measured using extinction co-efficients of 35,219 M^{-1} cm^{-1} for HSA [15]. The extinction coefficient of BSH (304 nm) was estimated from the absorbance slope against drug concentration, which was calculated to be 1982.239 M^{-1} cm^{-1}. The amount of drug bound to HSA (C_b) was calculated by subtracting the concentration of free drug from the total drug concentration. Binding parameters were determined using the Scatchard plot, where "r" represents the ratio of the bound drug to total HSA concentration and C_f is the concentration of the free drug. The intercept of the linear region of the binding curve on the x-axis represents the apparent number of binding sites (n). The negative slope of the curve corresponds to the apparent binding constant (K) [16], and the slope of Ln (r/nr) against Ln (C_f) determines the Hill coefficient value (nH).

2.8. Molecular docking protocol

The crystal structure of HSA (PDB ID:1AO6) was extracted from the manufacturer's database (http://www.pdb.org/pdb/home/home.do). Removal of water, the addition of some hydrogen atoms, and energy optimization of HSA were performed using UCSF Chimera 1.16 software. The BSH geometry was constructed and optimized using Chem3D Ultra 14.0 (CambridgeSoft.com). The optimized structure of BSH was ultimately utilized for molecular docking calculations.

In this study, the interactions between BSH and HSA were simulated using the semi-flexible docking method in AutoDock Vina (http://autodock.scripps.edu/) and BSH was considered to be a flexible molecule. The dimensions of the box were also set at 40 × 60 × 40 Å. Other parameters were maintained at default values. Finally, the best binding poses for the BSH-HSA complex were extracted from the docking results and analyzed using Discovery Studio 2021.

3. Results

3.1. UV–visible measurement

UV–vis spectroscopy is a beneficial method for detecting the interactions between proteins and small molecules. Typically, the position of the absorbance peak of a small molecule changes when it interacts with a protein to form a complex. In Fig. 1, the UV–vis spectra of HSA were examined in the absence (Fig. 1A) and presence (Fig. 1B) of BSH at the 280 nm peak position. Upon the addition of BSH to HSA, a decrease in absorption was observed. As BSH has significant absorbance in the 280 nm region, each BSH spectrum is subtracted from its corresponding BSH-HSA spectrum. Since, the exact mode of interaction between the two molecules cannot be determined solely from these data, further experiments might be necessary to gain a better understanding of these binding modes.

3.2. The mechanism of fluorescence quenching of HSA by BSH

As is well known, the intrinsic fluorescence of HSA is due to the presence of Trp and Tyr amino acids in its structure. However, the fluorescence intensity of the Trp residue is stronger and more sensitive to changes in the microenvironment. So, the binding of the drug to HSA affects the microenvironment around Trp, changes it, and affects its fluorescence intensity [17–19].
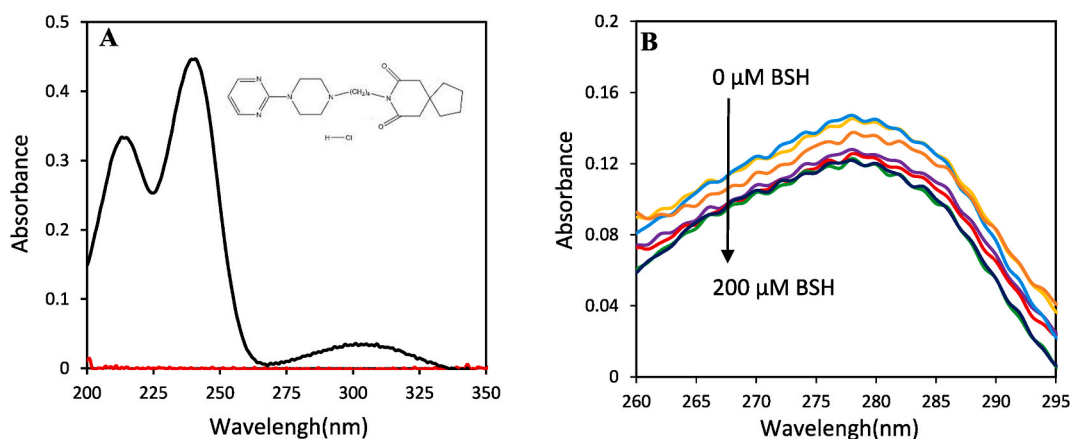

Fig. 1. (A) UV absorption spectrum of BSH (100 μM) in a buffer solution in 298 K. (B) Difference UV absorption spectra of HSA in the absence and presence of BSH at 298 K (Each BSH spectrum is subtracted from its corresponding BSH-HSA spectrum).

The fluorescence emission spectra of HSA were recorded by adding different amounts of BSH after excitation at 295 nm. As shown in Fig. 2A, the fluorescence intensity of HSA gradually decreased as the concentration of BSH increased, suggesting that BSH could interact with HSA and quench the intrinsic fluorescence intensity of Trp in HSA.

In general, the interaction between chromophore species in macromolecules and quencher species may result in fluorescence quenching. Macromolecule fluorescence quenching is commonly classified into three categories: the dynamic quenching, the static quenching, and the combination of the two [14]. The static quenching resulted from forming a ground-state complex between protein and quencher, the dynamic quenching resulted from the collision of protein and quencher, and combined dynamic and static quenching resulted from both collision and complex formation with the same quencher, respectively [17,20].

There are several methods to differentiate between static and dynamic quenching, such as comparing the values of the Stern-Volmer quenching constant (K_{sv}) and biomolecule quenching constant (K_q) at different temperatures. In the case of dynamic quenching, the Stern-Volmer constant (K_{sv}) exhibits a rise as the temperature increases, because an increase in temperature leads to faster quencher diffusion. In contrast, for static quenching, the K_{sv} value decreased with increasing temperature, because the stability of the complex diminished at higher temperatures [14]. Fig. 2B shows the Stern-Volmer diagram. Stern-Volmer Eq. (2) [18]:

$$\frac{F_0}{F} = 1 + K_{sv}[Q] = 1 + K_q \tau_0 [Q] \tag{2}$$

where F and F_0 are the fluorescence intensities in the presence and absence of the quencher, respectively. According to the information obtained from the Stern-Volmer diagram and the decreasing slope of the diagram, it can be seen that the mechanism of HSA quenching after interaction with the BSH is dynamic. In order to further investigate the quenching mechanism, the bimolecular quenching constant (K_q) was determined using the equation $K_q = K_{sv}/\tau_0$. Here τ_0 is the average lifetime of a biomolecule without a quencher, which is 10^{-8} s [21].

Table 1 displays the K_{sv} and K_q values, which exhibit an increase with elevated temperature. Also considering that the maximum bimolecular quenching constant (K_q) of various quenchers with biopolymers is usually 2.0×10^{10} M^{-1} s^{-1} [22] and K_q values obtained here are more than this value, it can be concluded that the HSA quenching mechanism by BSH is not only dynamic quenching [23]. Therefore, the quenching mechanism of HSA caused by BSH was identified as a mixed quenching.

The number of bindings per albumin (n) and binding constant (K_b) was calculated from Eq. (3):
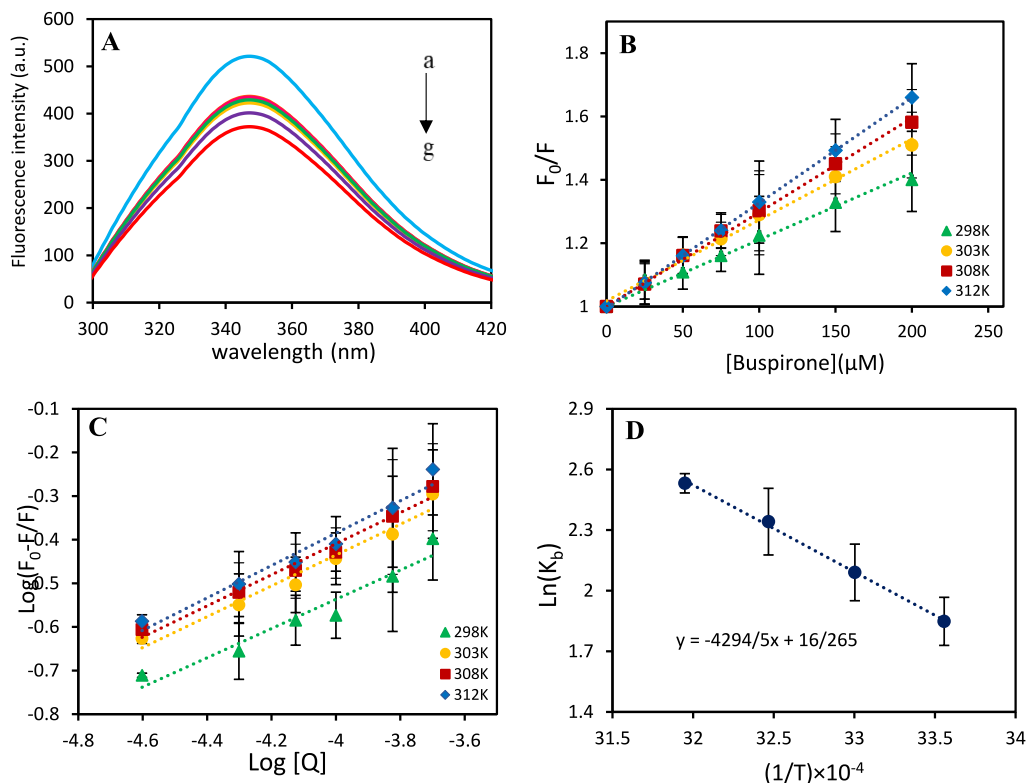

Fig. 2. (A) Effect of various concentrations of BSH (a-g; 0, 25, 50, 75, 100, 150, and 200 μM) on HSA (5 μM) in 298 K. (B) Stern-Volmer plot for determination of the quenching rate constant of BSH on HSA. (C) Plot of log (F$_0$–F)/F against log Q for BSH-HSA interaction. (D) Van't Hoff plot for the binding interaction between BSH and HSA.

$$\log \frac{F_0 - F}{F} = \log K_b + n\log [Q] \tag{3}$$

The modified Stern-Volmer plots at different temperatures are shown in Fig. 2C The values of n and K_b were calculated as the slopes and intercept of the double-logarithm curves by using the above equation and Fig. 2C. The value of n shows that the interaction of ligands with protein is cooperative or non-cooperative in nature. The outcomes displayed the n values were all near one in the studied temperature, suggesting that BSH may just occupy one binding site on HSA.

The value of K_b indicates the distribution of the drug in plasma, weak binding indicates poor distribution or short lifetime, while strong binding indicates a decrease in free drug concentration in plasma. According to Table 1, BSH shows small binding constants compared to most albumin ligands such as ibuprofen, warfarin, indomethacin, or digitoxin (10^6 M^{-1}) [24–26]. It was also found that the values of K_b increase with increasing temperature, which is in line with the dependence of K_{sv} on temperature and the stability of the BSH-HSA complex.

3.3. Thermodynamic parameters and determination of the type of interactions

Ligand binding to macromolecules typically involves four main interactions: hydrogen bonding, van der Waals forces, hydrophobic interactions, and electrostatic forces. $\Delta H° > 0$ and $\Delta S° > 0$ correspond to hydrophobic forces; $\Delta H° < 0$ and $\Delta S° < 0$ correspond to van der Waals interaction and hydrogen-bond formation; $\Delta H° < 0$ and $\Delta S° > 0$ correspond to electrostatic/ionic forces. Therefore, in the present study, thermodynamic parameters were examined to determine the effective forces in the interaction between BSH and HSA. By plotting the binding constants obtained at different temperatures (298, 303,308 and 312 K) by the Van't Hoff Eq. (Fig. 2D), thermodynamic parameters were also calculated using equations (4) and (5), and the results are shown in Table 2.

$$\ln K_b = \frac{-\Delta H°}{RT} + \frac{\Delta S°}{R} \tag{4}$$

$$\Delta G° = \Delta H° - T\Delta S° = -RT\ln K \tag{5}$$

where R is the gas constant and K_b is the binding constant at the respective temperatures. According to the information in Table 2, $\Delta H°$ and $\Delta S°$ in the interaction between BSH and HSA are negative. Based on the viewpoint of Ross and Subramanian [27], the positive value of $\Delta H°$ and $\Delta S°$ indicates that the main driven forces in the BSH-HSA system are hydrophobic forces. In addition, the results showed that the binding process of BSH to HSA was spontaneous due to the negative values of ΔG in the studied temperature range [28]; so, it can be concluded that the formation of stable BSH-HSA complexes might be easy.

3.4. Energy transfer from HSA to BSH

Förster resonance energy transfer (FRET) is commonly employed to determine the distance between a donor and acceptor molecule [18]. Its wide applications include the analysis of interactions between biological macromolecules, immunoassays, and research on cell physiology. The energy transfer from the donor to the acceptor can be estimated when the following conditions are met [29]: (a) the donor spectrum overlaps with the spectrum of the acceptor, (b) the chromophores are arranged appropriately, and (c) the maximum distance between the donor and acceptor is 8 nm. The values of energy transfer efficiency (E), distance (r), and overlap integral between the emission and absorbance spectra (J) can be calculated using FRET with the help of equations (6)–(8) [14]:

$$E = 1 - \frac{F}{F_0} = \frac{R_0^6}{R_0^6 + r^6} \tag{6}$$

$$R_0 = 0.2108 \times \left[k^2 \times \Phi_D \times n^{-4} \times J(\lambda)\right]^{1/6} \tag{7}$$

$$J(\lambda) = \int_0^\infty F_D(\lambda) \times \varepsilon_A(\lambda) \times \lambda^4 \times d\lambda \tag{8}$$

The emission spectrum of HSA and The UV spectrum of BSH are shown in Fig. 3 (a and b). The values of the different parameters were calculated by the relevant equations. The R_0 value, which indicates the Förster distance at an energy transfer efficiency of 50 %, was found to be 2.91 nm. The distance between the donor and acceptor molecules (r) was determined to be 3.61 nm, which was less than the maximum distance required for energy transfer (8 nm). The energy transfer efficiency (E) was calculated to be 21.75 %, and

Table 1
The Stern-Volmer quenching constant (K_{sv}) for the interaction of BSH and HSA at three distinct temperatures.

pH	T(K)	$K_{sv} \times 10^3$ (M^{-1})	$K_q \times 10^{12}$ (L mol^{-1} s^{-1})
7.4	298	1.99 ± 0.23	0.199
	303	2.55 ± 0.26	0.255
	308	2.97 ± 0.28	0.297
	312	3.32 ± 0.19	0.332

Table 2

Binding and thermodynamic parameters of HSA–BSH. The data are the means ± standard deviations of three independent.

T(K)	Log K_b	$\Delta S°$ (J mol^{-1} K^{-1})	$\Delta H°$ (kJ mol^{-1})	$\Delta G°$ (kJ mol^{-1})
298	0.80 ± 0.016	135.23 ± 3.21	35.70 ± 2.65	−4.593
303	0.98 ± 0.019			−5.269
308	1.02 ± 0.015			−5.945
312	1.09 ± 0.021			−6.622

the overlap integral area (J(λ)) was also determined to be $4.48 \times 10^{+8}$ M^{-1} cm^{-1} nm^4. These values satisfy condition 0.5 $R_0 < r < 1.5$ R_0, indicating that the energy transfer between HSA and BSH occurs mainly through non-radiative means. Additionally, the result of $R_0 < r$ suggests that BSH quenched the fluorescence of HSA mainly through static quenching.

3.5. Structural changes of HSA

In order to gain a deeper understanding of the changes in the structure of HSA after interaction with BSH, the CD spectra of HSA and the BSH-HSA complex were measured. The CD spectra of HSA, with and without BSH, are shown in Fig. 4. The CD spectrum of HSA exhibits two negative regions at 208 and 222 nm, which correspond mainly to the α-helix in HSA [30]. Molar ellipticity decreased with the addition of BSH to the HSA solution, demonstrating that the binding of BSH to HSA induces conformational changes in the protein. The CD results are expressed as molar ellipticity ([θ]), which was calculated by the following Eq. (9):

$$[\theta] = \frac{\theta_{obs}}{10 n l c_p} \tag{9}$$

where θ is the absorbance in mdeg, n is the number of HSA amino acid residues, l is the cell path length (0.1 cm), and C_p is the mole fraction. The α helix content was determined from the [θ] values at 208 nm by following Eq. (10) [31]:

$$\alpha - \text{helix}\% = \left(\frac{-[\theta]_{208} - 4000}{33000 - 4000} \right) \times 100 \tag{10}$$

The changes in the secondary structure of HSA after interaction with BSH are shown in Table 3, showing that increasing the molar ratio of BSH to HSA increases the α-helix content from 63.88 % to 75.92 %.

The FT-IR results were used to further investigate the interaction between BSH and HSA, and the secondary structural changes in HSA. The amide bands in the FT-IR spectra of proteins represent various peptide vibrations and the number of amide bands. Amides I and II are related to the secondary structure of the proteins. Secondary structural changes significantly affect the amide I band more than the amide II band [14]. Typically, the spectral range of 1600–1700 cm^{-1} of amide I bands can be attributed to the α-helix, which is related to the carbonyl (C)O stretching vibrations [8]. Changes in the protein structure were characterized by changes in the position of the amide I band, as shown in Fig. 5(A-C). The changes in the position and shape of the amide I peak indicate that BSH binds to the carbonyl group of HSA and causes slight changes in the secondary structure of HSA, which is consistent with the CD findings.

3.6. Cooperative binding of BSH to HSA

Equilibrium dialysis was performed to understand the interactions between BSH and HSA. Dialysis involves the separation of particles in a liquid on the basis of differences in their ability to pass through a porous membrane. The porous membrane of the dialysis bag with a cut-off of 10 KD does not allow the protein weighing 66.5 KD to pass through, but it allows the BSH to pass between the two holders, in this way, after the time, the drug can be freely exchanged between the two sites and bind to the HSA [32]. Fig. 6A shows a
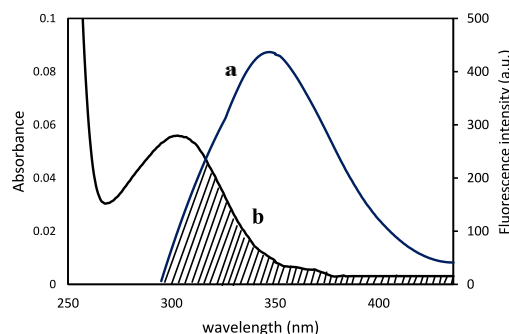

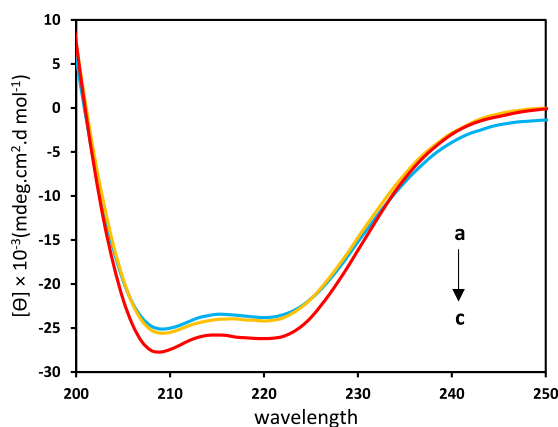**Fig. 3.** The overlap of (a) fluorescence spectrum of HSA (5 μM) with (b) UV spectrum of buspirone (25 μM).

Fig. 4. The CD spectra of HSA upon addition of varying concentrations of BSH in PBS at pH 7.4 ; (a–c) 0, 6.25, 12.5 μM and HSA (2 μM).

Table 3
Conformational composition of HSA before and after interaction with different BSH concentrations.

Secondary structures	HSA (2 μM)	6.25 μM	12.5 μM
α-Helix	63.88 %	70.13 %	75.92 %
β-Antiparallel	1.61 %	0.39 %	0.19 %
β-Turn	12.17 %	10.31 %	8.8 %
Random coil	19.42 %	15.07 %	11.54 %

Scatchard plot showing a cooperative binding pattern for BSH with a positive slope at low r-values of the binding isotherm. Fig. 6B shows a plot of r versus C_f (concentration of free drug). The plot demonstrates an initial increase in r as C_f increases, followed by a decrease in slope, which reflects the approach of the system towards equilibrium or saturation [33]. When Ln r/n-r was plotted against Ln C_f, a straight line was obtained with a Hill coefficient (nH) of 1.69, confirming a positive cooperativity (Fig. 6C) [32]. The binding constant was determined to be 0.15×10^2 M^{-1}. Also, the negative ΔG value indicated that the binding of the drug to the protein was spontaneous. The binding isotherms are presented in Table 4.

3.7. Molecular docking results

The AutoDock Vina program was used with a maximum number of supported runs to determine the most likely binding mode of BSH in the HSA active site. After examining the obtained binding results, the binding mode with the lowest energy, was selected in interaction with IIA, IIIA, and IIB subunits of HSA. Considering that Trp-214 in the HSA structure is located near subunit IIA [34,35], as shown in Fig. 7, it can be seen that BSH interacts with Trp-214, which is consistent with the experimental results.

The hydrophobic regions of BSH interacted with Trp-214, Arg-218, Ile-264, Ile-290, and Tyr-452, which were found in the hydrophobic binding pocket (Figs. 7A and 8B). It can be concluded that hydrophobicity is one of the most significant interactions between BSH and HSA, which is consistent with the thermodynamic parameters calculated in the previous sections. Additionally, hydrogen bonding with Lys-195 and Lys-199 may have occurred during this interaction, contributing to the stability of the BSH-HSA complex. All these interactions are listed in Table 5. Fig. 8 provides an overview of the interactions between buspirone and amino acids present in HSA.

4. Discussion

To sum up, the interaction between BSH and HSA using different techniques including UV–vis spectroscopy, fluorescence emission, Circular Dichroism, FT-IR, equilibrium dialysis, and molecular docking was studied. The UV–vis and fluorescence spectroscopy results confirmed the interaction between BSH and HSA. Also, fluorescence emission spectra revealed that BSH effectively quenched the intrinsic fluorescence of HSA under physiological conditions through a combination of dynamic and static quenching. Furthermore, the Scatchard diagram and Hill equation showed positive cooperative binding of BSH to HSA. Based on CD and FT-IR spectroscopy, we came to this point that conformational changes occurred in HSA upon interaction with BSH, which is consistent with the results obtained for other antidepressants and anxiolytics such as sertraline and bupropion [25,36]. Moreover, molecular docking demonstrated that BSH binds to HSA with a favorable binding score and this binding occurs spontaneously. It was also found that HSA interacts with subdomains IIA, IIIA, and IIB, which is consistent with the results obtained from molecular docking of other antidepressants such as biperiden, haloperidol, and clonazepam [37]. However, considering the high binding tendency of warfarin and bilirubin to bind to subdomain IIA, as well as the high tendency of digitoxin and ibuprofen to bind to subdomain IIIA compared to BSH,
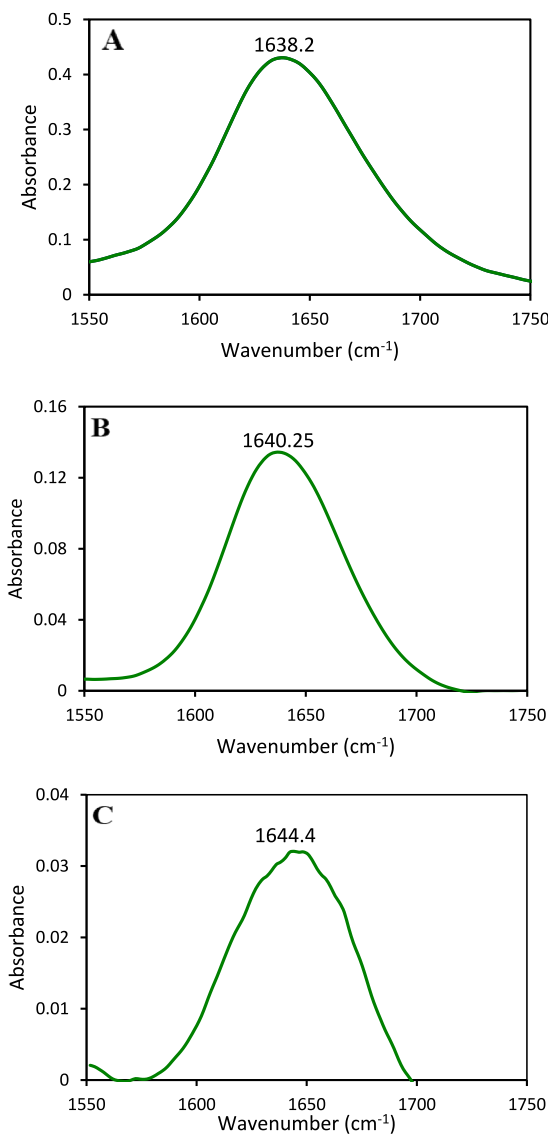
Fig. 5. FT-IR spectra of HSA in the absence and presence of different concentrations of BSH in a buffer solution. (A) FT-IR spectrum of free HSA (100 μM) (B) FT-IR difference spectrum (subtracting the absorption of the BSH free form that HSA–BSH) [HSA]: [BSH] = 1:0.5. (C) [HSA]: [BSH] = 1:1.

the probability of these compounds binding to these sites on HSA is higher than BSH [38].

Overall, the present study can provide useful information regarding the specific binding sites and types of interactions between BSH and HSA under physiological conditions. It may also improve our understanding of the effects of this drug on HSA function and may help in designing more effective drugs with higher clinical efficacies. Conclusions from the experiment results can be drawn as follows:

a. BSH can effectively quench the endogenous fluorescence of HSA by combining dynamic and static quenching mechanisms, and the fluorescence quenching of HSA is mainly caused by the complex formation of HSA with BSH. $\Delta S°$ and $\Delta H°$ positive values suggest dynamic involvement of the hydrophobic interactions during HSA's fluorescence quenching with buspirone.
b. The binding site is approximately equal to 1, suggesting that BSH may just occupy one binding site on HSA.
c. The main interaction forces in the binding process of BSH with HSA are hydrophobic forces, which are similar to the results obtained from the interaction of BSH with BSA (BSA is a protein with high structural and functional similarity with HSA) [39].
d. According to these in vivo and in vitro studies, buspirone is highly protein bound (more than 95 %) and interacts with albumin and alpha acid glycoprotein. However, the results of clinical studies showed that buspirone did not displace propranolol, digoxin, or warfarin from plasma proteins [40].
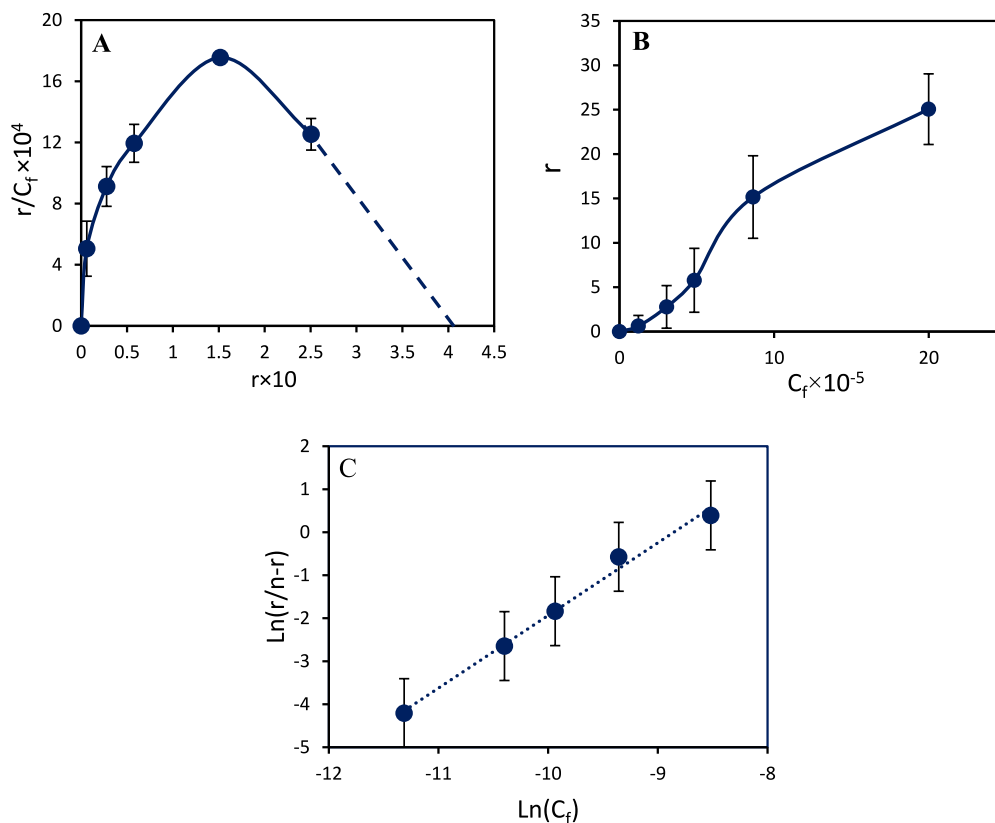
Fig. 6. (A) Plot of r values against free BSH. (B) Scatchard plots of BSH binding to HSA. [BSH] = 0, 25, 50, 75, 150, 300 μM and [HSA] = 3 μM (C) Plot of the Hill equation for the binding of BSH to HSA.

Table 4
Binding parameters for BSH interaction with HSA
The data are the means ± standard deviations of three independent.

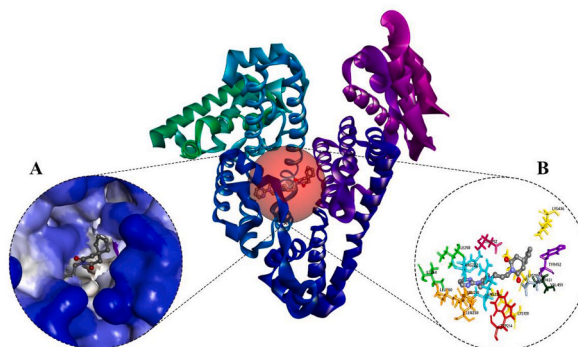| T(K)	K_b (M^{-1})	nH	ΔG° (kJ/mol)
297 ± 2	15 ± 0.45	1.69 ± 0.045	−6.70

Fig. 7. The optimal binding configuration of the BSH-HSA complex (A) Magnified view of BSH within the hydrophobic pocket of HSA for BSH in the hydrophobic pocket of HSA. (B) Schematic representation of hydrophobic and hydrogen bonds between BSH and nearby residues on HSA at the binding site.
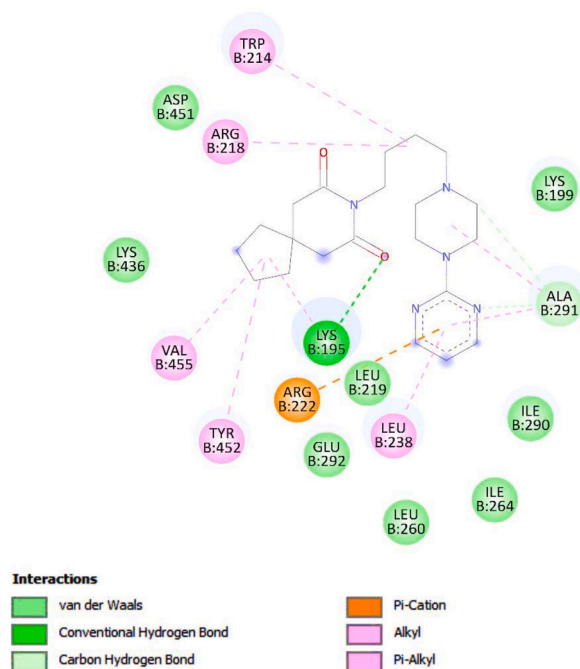
Fig. 8. 2D diagram of BSH and HSA interactions.

Table 5
The type of interaction of BSH with its adjacent amino acids.

Type of interaction	Residue	Distance (Å)
Hydrogen Bonds	Lys-195	2.75
	Lys-199	2.53
	Lys-195	4.00
Hydrophobic Interactions	Trp-214	3.79
	Trp-214	3.57
	Arg-218	3.77
	Ile-264	3.97
	Ile-290	3.64
	Tyr-452	3.64
	Tyr-452	3.51

Data availability

Data will be made available on request.

CRediT authorship contribution statement

Javad Sargolzaei: Writing – review & editing, Visualization, Supervision, Methodology, Funding acquisition, Formal analysis, Data curation, Conceptualization. **Elaheh Jalali:** Writing – original draft, Validation, Software, Investigation, Formal analysis, Data curation. **Parisa Rajabi:** Writing – review & editing, Writing – original draft, Visualization, Software.

Declaration of competing interest

The authors declare that they have no known competing financial interests or personal relationships that could have appeared to influence the work reported in this paper.

Acknowledgments

References

[1] M.A. Zayed, A.A. El-Habeeb, Spectroscopic study of the reaction mechanism of buspirone interaction with iodine and tetracyanoethylene reagents and its applications, Drug Test. Anal. 1 (6) (2009) 267–274.

[2] A. Jaipal, M.M. Pandey, S.Y. Charde, P.P. Raut, K. V Prasanth, R.G. Prasad, Effect of HPMC and mannitol on drug release and bioadhesion behavior of buccal discs of buspirone hydrochloride: in-vitro and in-vivo pharmacokinetic studies, Saudi Pharmaceut. J. 23 (3) (2015) 315–326.

[3] A.S. Eison, D.L. Temple Jr., Buspirone: review of its pharmacology and current perspectives on its mechanism of action, Am. J. Med. 80 (3) (1986) 1–9.

[4] C. Loane, M. Politis, Buspirone: what is it all about? Brain Res. 1461 (2012) 111–118.

[5] T.A. Wani, A.H. Bakheit, S. Zargar, S. Alamery, Mechanistic competitive binding interaction study between olmutinib and colchicine with model transport protein using spectroscopic and computer simulation approaches, J. Photochem. Photobiol. Chem. 426 (2022) 113794.

[6] P. Lee, X. Wu, Modifications of human serum albumin and their binding effect, Curr. Pharmaceut. Des. 21 (14) (2015) 1862–1865.

[7] T.A. Wani, S. Zargar, A. Hussain, Spectroscopic, thermodynamic and molecular docking studies on molecular mechanisms of drug binding to proteins, Molecules 27 (23) (2022) 8405. MDPI.

[8] M. Shahlaei, B. Rahimi, A. Nowroozi, M.R. Ashrafi-Kooshk, K. Sadrjavadi, R. Khodarahmi, Exploring binding properties of sertraline with human serum albumin: combination of spectroscopic and molecular modeling studies, Chem. Biol. Interact. 242 (2015) 235–246.

[9] R. Beauchemin, C.N. N'Soukpoe-Kossi, T.J. Thomas, T. Thomas, R. Carpentier, H.A. Tajmir-Riahi, Polyamine analogues bind human serum albumin, Biomacromolecules 8 (10) (2007) 3177–3183.

[10] S. Zargar, T.A. Wani, N.A. Alsaif, A.I.A. Khayyat, A comprehensive investigation of interactions between antipsychotic drug quetiapine and human serum albumin using multi-spectroscopic, biochemical, and molecular modeling approaches, Molecules 27 (8) (2022) 2589.

[11] G. Fanali, A. Di Masi, V. Trezza, M. Marino, M. Fasano, P. Ascenzi, Human serum albumin: from bench to bedside, Mol. Aspect. Med. 33 (3) (2012) 209–290.

[12] P. Ascenzi, M. Fasano, Allostery in a monomeric protein: the case of human serum albumin, Biophys. Chem. 148 (1–3) (2010) 16–22.

[13] T. Peters Jr., All about Albumin: Biochemistry, Genetics, and Medical Applications, Academic press, 1995.

[14] Y.-F. Zhang, K.-L. Zhou, Y.-Y. Lou, D. Pan, J.-H. Shi, Investigation of the binding interaction between estazolam and bovine serum albumin: multi-spectroscopic methods and molecular docking technique, J. Biomol. Struct. Dyn. 35 (16) (2017) 3605–3614.

[15] N. Shahabadi, M. Razlansari, Exploring the interaction of nanocomposite composed of Fe3O4, CaAl layered double hydroxide and lamivudine drug with Human serum albumin (HSA): spectroscopic studies, J. Nanoanal. 5 (2) (2018) 106–114.

[16] G. Scatchard, The attractions of proteins for small molecules and ions, Ann. N. Y. Acad. Sci. 51 (4) (1949) 660–672.

[17] Q. Wang, et al., Binding interaction of atorvastatin with bovine serum albumin: spectroscopic methods and molecular docking, Spectrochim. Acta Mol. Biomol. Spectrosc. 156 (2016) 155–163.

[18] J.R. Lakowicz, Principles of Fluorescence Spectroscopy, Springer, 2006.

[19] Y. Moriyama, D. Ohta, K. Hachiya, Y. Mitsui, K. Takeda, Fluorescence behavior of tryptophan residues of bovine and human serum albumins in ionic surfactant solutions: a comparative study of the two and one tryptophan (s) of bovine and human albumins, J. Protein Chem. 15 (1996) 265–272.

[20] J. Shi, D. Pan, M. Jiang, T.-T. Liu, Q. Wang, Binding interaction of ramipril with bovine serum albumin (BSA): insights from multi-spectroscopy and molecular docking methods, J. Photochem. Photobiol., B 164 (2016) 103–111.

[21] U. Katrahalli, S. Jaldappagari, S.S. Kalanur, Probing the binding of fluoxetine hydrochloride to human serum albumin by multispectroscopic techniques, Spectrochim. Acta Mol. Biomol. Spectrosc. 75 (1) (2010) 314–319.

[22] D.P. Yeggoni, A. Rachamallu, R. Subramanyam, Protein stability, conformational change and binding mechanism of human serum albumin upon binding of embelin and its role in disease control, J. Photochem. Photobiol., B 160 (2016) 248–259.

[23] T.A. Wani, A.H. Bakheit, S. Zargar, A.I.A. Khayyat, A.A. Al-Majed, Influence of rutin, sinapic acid, and naringenin on binding of tyrosine kinase inhibitor erlotinib to bovine serum albumin using analytical techniques along with computational approach, Appl. Sci. 12 (7) (2022) 3575.

[24] S. Evoli, D.L. Mobley, R. Guzzi, B. Rizzuti, Multiple binding modes of ibuprofen in human serum albumin identified by absolute binding free energy calculations, Phys. Chem. Chem. Phys. 18 (47) (2016) 32358–32368.

[25] M. Shahlaei, B. Rahimi, A. Nowroozi, M.R. Ashrafi-Kooshk, K. Sadrjavadi, R. Khodarahmi, Exploring binding properties of sertraline with human serum albumin: combination of spectroscopic and molecular modeling studies, Chem. Biol. Interact. 242 (2015) 235–246.

[26] H. Olsen, A. Andersen, A. Nordbø, U.E. Kongsgaard, O.P. Børmer, Pharmaceutical-grade albumin: impaired drug-binding capacity in vitro, BMC Clin. Pharmacol. 4 (2004) 1–9.

[27] P.D. Ross, S. Subramanian, Thermodynamics of protein association reactions: forces contributing to stability, Biochemistry 20 (11) (1981) 3096–3102.

[28] P. Chen, et al., Comparison of the binding interactions of 4-hydroxyphenylpyruvate dioxygenase inhibitor herbicides with humic acid: insights from multispectroscopic techniques, DFT and 2D-COS-FTIR, Ecotoxicol. Environ. Saf. 239 (2022) 113699.

[29] B.-L. Wang, S.-B. Kou, Z.-Y. Lin, J.-H. Shi, Investigation on the binding behavior between BSA and lenvatinib with the help of various spectroscopic and in silico methods, J. Mol. Struct. 1204 (2020) 127521.

[30] W. He, Y. Li, J. Liu, Z. Hu, X. Chen, Specific interaction of chalcone-protein: cardamonin binding site II on the human serum albumin molecule, Biopolym.: Orig. Res. Biomol. 79 (1) (2005) 48–57.

[31] Z.X. Lu, T. Cui, Q.L. Shi, Applications of circular dichroism and optical rotatory dispersion in molecular biology, Science (1987) 79–82. Beijing.

[32] A.V. Hill, The possible effects of the aggregation of the molecules of hemoglobin on its dissociation curves, J. Physiol. 40 (1910) iv–vii.

[33] L.S. Clegg, W.E. Lindup, Scatchard plots with a positive slope: dependence upon ligand concentration, J. Pharm. Pharmacol. 36 (11) (1984) 776–779.

[34] Y. Wang, L. Wang, M. Zhu, J. Xue, R. Hua, Q.X. Li, Comparative studies on biophysical interactions between gambogic acid and serum albumin via multispectroscopic approaches and molecular docking, J. Lumin. 205 (2019) 210–218.

[35] L. Wang, et al., Multi-spectroscopic measurements, molecular modeling and density functional theory calculations for interactions of 2, 7-dibromocarbazole and 3, 6-dibromocarbazole with serum albumin, Sci. Total Environ. 686 (2019) 1039–1048.

[36] M. Manjushree, H.D. Revanasiddappa, Interpretation of the binding interaction between bupropion hydrochloride with human serum albumin: a collective spectroscopic and computational approach, Spectrochim. Acta Mol. Biomol. Spectrosc. 209 (2019) 264–273.

[37] C.P. de Morais Coura, V.M. da Silva Fragoso, E.C.N. Valdez, E.T. Paulino, D. Silva, C.M. Cortez, Study on the interaction of three classical drugs used in psychiatry in albumin through spectrofluorimetric modeling, Spectrochim. Acta Mol. Biomol. Spectrosc. 255 (2021) 119638.

[38] Y.-C. Chen, H.-M. Wang, Q.-X. Niu, D.-Y. Ye, G.-W. Liang, Binding between saikosaponin C and human serum albumin by fluorescence spectroscopy and molecular docking, Molecules 21 (2) (2016) 153.

[39] V. Patil, S. Labade, C. Khilare, S. Sawant, A molecular bridge-like binding mode of buspirone to BSA: multispectroscopic and molecular docking investigation, Chem. Data Collect. 40 (2022) 100892.

[40] R.E. Gammans, R.F. Mayol, J.A. Labudde, Metabolism and disposition of buspirone, Am. J. Med. 80 (3) (1986) 41–51.